ACS APPLIED MATERIALS & INTERFACES

Research Article

www.acsami.org

Electrochemical Preparation of Photosystem I–Polyaniline Composite Films for Biohybrid Solar Energy Conversion

Evan A. Gizzie,[†] Gabriel LeBlanc,[†,§] G. Kane Jennings,[‡] and David E. Cliffel*[,†]

[†]Department of Chemistry, Vanderbilt University, Nashville, Tennessee 37235-1822, United States

[‡]Department of Chemical and Biomolecular Engineering, Vanderbilt University, Nashville, Tennessee 37235-1604, United States

Supporting Information

ABSTRACT: In this work, we report for the first time the entrapment of the biomolecular supercomplex Photosystem I (PSI) within a conductive polymer network of polyaniline via electrochemical copolymerization. Composite polymer–protein films were prepared on gold electrodes through potentiostatic electropolymerization from a single aqueous solution containing both aniline and PSI. This study demonstrates the controllable integration of large membrane proteins into rapidly prepared composite films, the entrapment of such proteins was observed through photoelectrochemical analysis. PSI's unique function as a highly efficient biomolecular photodiode generated a significant enhancement in photocurrent generation for the PSI-loaded polyaniline films, compared to pristine polyaniline films, and dropcast PSI films. A comprehensive study was then performed to separately evaluate film thickness and PSI concentration in the initial polymerization solution and their effects on the net photocurrent of this novel material. The best performing composite films were prepared with 0.1 μM PSI in the polymerization solution and deposited to a film thickness of 185 nm, resulting in an average photocurrent density of 5.7 μA cm^{-2} with an efficiency of 0.005%. This photocurrent output represents an enhancement greater than 2-fold over bare polyaniline films and 200-fold over a traditional PSI multilayer film of comparable thickness.

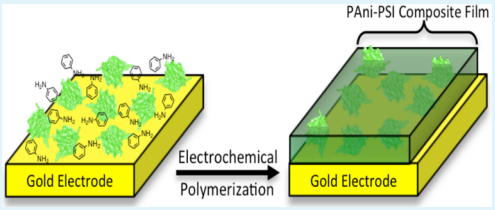

KEYWORDS: *biocomposite materials, solar energy conversion, biohybrid solar cells, conjugated polymers*

INTRODUCTION

Photosystem I (PSI) is one of the key enzymatic components of photosynthesis in green plants and other autotrophs. Billions of years of environmental stimuli have evolved this ~500 kDa protein supercomplex into nature's most efficient photodiode, with in vivo charge separation efficiency near unity.[1−3] Along with its vast natural abundance, ease of extraction, and robustness, PSI has attracted significant attention from researchers who aim to integrate the protein into highly efficient, biohybrid solar energy conversion devices.[4,5] This field of research is based upon the need to construct biohybrid electrodes and ultimately stand-alone photovoltaic devices utilizing the biological material, PSI, as the principle photoactive component. As opposed to current, state-of-the-art photovoltaics such as semiconductor photodiodes or dye-sensitized solar cells, PSI-derived devices offer advantages such as low cost, readily abundant materials, simple processing, and scalability. For these reasons, the PSI-based photovoltaics have been widely researched in recent decades as sustainable solar energy conversion alternatives to traditional solar avenues.[5]

Early work with PSI relied on solution-phase self-assembly of the protein on functionalized gold electrodes.[6−8] In subsequent work, the manual drop-casting of thick protein films on gold substrates proved to enhance the photocurrent yields of biohybrid PSI electrodes. By increasing the overall protein loading on the surface of the electrode, multilayer PSI assemblies on traditional electrode materials are capable of achieving photocurrent densities that are significantly larger than those observed from single PSI monolayers. Current densities for PSI multilayer assemblies are often observed in the μA cm^{-2} regime;[9] however, performances are limited by competing electrochemical processes of non-specifically oriented proteins in drop-cast films.[10] Moving forward in the development of the "next-generation" biohybrid photovoltaic materials, it is of extreme importance to improve the interfacial electron transfer pathways. Thus, in this work, a photoactive composite material that fully incorporates PSI as its active component is constructed to facilitate the electron transfer from enzyme to electrode while circumventing the issues of poor electron transfer, aggregation and orientation. Improving the electron transfer pathways, from enzyme to electrode, is of extreme importance in development and further enhancement of biophotovoltaic devices.

The concept of immobilizing photosystem enzymes on polymer-functionalized electrodes has demonstrated improved electron transfer by directing electron flow from enzyme to electrode through the conductive film.[11,12] Incorporating the protein into a redox-active polymer network has attracted significant attention, due to improved electron transfer, increased enzyme loading in the three dimensional network, de-emphasis on uniform protein orientation, and extension of enzyme lifetime.[13] Redox-active hydrogels constructed from

Received: July 9, 2014
Accepted: April 21, 2015
Published: April 21, 2015

DOI: 10.1021/acsami.5b01065
ACS Appl. Mater. Interfaces 2015, 7, 9328−9335

poly(*n*-vinylimidazole) backbones loaded with transition metal complexes (i.e., osmium-bis(2,2′-bipyridine)dichloride) have been utilized for the immobilization of PSI,[14] and also for PSII,[15] with both cases producing photocurrent densities that greatly surpassed the previous performance of protein multilayers on gold. Loading hydrogels with transition metal complexes of osmium, ruthenium, or cobalt significantly enhances the electron diffusion coefficients through the film.[16] However, metal coordination compounds (specifically that of osmium) are very costly to prepare and thus are not a viable solution for scalable biohybrid, solar energy technologies. Additionally, two recent publications have demonstrated the utility of polymer-immobilized PSI devices.[17,18] However, in each case, drawbacks exist from costly materials and/or extensive processing, thus these emerging technologies prohibitively lack scalability. In this work, carbon-based polymers are explored as conductive matrices for the immobilization of PSI, to expand upon recent advances in PSI composite materials.

Aside from redox-active hydrogels, there exists a class of intrinsically conductive polymers, which are categorized by their π-conjugated backbones. Polyaniline (PAni) is one such material known specifically for its low cost, high conductivity, environmental stability, and ease of electrochemical preparation under mild aqueous conditions.[19] Other enzymes, such as glucose oxidase, have been successfully incorporated into electroactive polymers (via an electropolymerization mechanism) for use in highly specific biosensors.[20,21] Thus, we have theorized that entrapment of PSI within a conductive PAni network is possible through coelectropolymerization aided by hydrogen bonding between aniline oligomers and various amino acid residues.

In this work, composite PAni−PSI films were prepared via electropolymerization from a single solution containing both aniline and PSI. These composite films were then evaluated electrochemically to verify the entrapment of PSI in the PAni network, and the retention of enzymatic activity following the entrapment process. The optimized PAni−PSI composites in this study produced an external quantum efficiency near 0.005%, which is comparable to first-generation PSI multilayers. However, these newly developed PAni−PSI composites were 10-fold thinner and contained 70-fold less protein material than a traditional drop-cast PSI multilayer film. Based on the successful incorporation of an active and functioning form of the protein supercomplex, the scope of this work extends far beyond the construction of photoactive composites for photovoltaic applications. To our knowledge, this is the first instance of successful integration of very large (>500 kDa) biomolecules, specifically integral membrane proteins, into polymer films via a rapid, controllable, surfactant-stabilized coelectropolymerization from aqueous media. The applications of this processing extend into other arenas of bionanotechnology, biomaterials, and biosensing.

EXPERIMENTAL SECTION

Isolation of Photosystem I. Photosystem I was extracted and isolated using methods described elsewhere,[6] with minor procedural modifications. In short, ∼200 g of baby spinach leaves were deveined and macerated. This extract was centrifuged (8000*g* for 1 min) in order to precipitate the chloroplasts. This pellet was resuspended in a small volume (∼20 mL) of buffer containing Triton X-100 (Acros Organic) surfactant to lyse the thylakoid membrane bilayer. This suspension was then centrifuged again (20000*g* for 15 min) precipitating all insoluble plant matter. The supernatant was then purified using a hydroxylapitite (EMD Millipore) column as described previously by Shiozawa et al.,[22] resulting in purified PSI supercomplexes eluted in 0.2 M phosphate buffer (pH = 7.00) with 0.05% (w/v) Triton X-100.

The PSI samples were then dialyzed (10 kDa MWCO) against 20 mM phosphate buffer pH = 7.00 to remove the excess buffer salts. Following dialysis, this PSI stock was characterized using spectrophotometric methods devised previously by Baba et al.,[23] with the exception of the electron donor used in the determination of P700 concentration, which was dithiothreitol (Fisher). Stock PSI samples were aliquoted into individual P700 concentrations of 1.6 μM and stored at −80 °C for later use.

Electrode Preparation and Modification. For all electrochemical experiments, PAni and PAni−PSI composite films were deposited on 2 mm gold disk electrodes (area = 0.031 cm^2), which were first polished using a series of alumina powder slurries from 1 to 0.05 μm in order to obtain a smooth electrode surface, which was confirmed with an optical microscope (Olympus BX41) at 500× magnification. After polishing, the electrodes were sonicated in distilled water for a minimum of 15 min to remove any alumina powder adsorbed on the gold surface.

For film thickness and PSI quantification experiments, gold wafer electrodes were used. These electrodes were prepared by thermally evaporating 125 nm of gold on silicon substrates (⟨100⟩ orientation) with a 10 nm adhesion layer of chromium. Au/Si substrates were cut to a working area of 1 cm^2 for film depositions.

For film preparation, electropolymerization was performed using a CH Instruments 660A electrochemical workstation three-electrode setup with a platinum mesh counter electrode and Ag/AgCl (3 M KCl) reference electrode.

For the evaluation of the polymerization time−photocurrent relationship, the PAni−PSI composite films were prepared in 1 M aniline (Fisher), 0.941 M HCl (Fisher), 4 mM sodium phosphate (Fisher), 0.3 μM PSI, and 0.01% (w/v) Triton X-100. The PAni control films were prepared in 1 M aniline, 0.941 M HCl, 4 mM sodium phosphate, and 0.01% (w/v) Triton X-100. At a fixed electropolymerization potential (+1.2 V vs Ag/AgCl) the deposition time was modulated between 10 and 120 s, resulting in an array of film thicknesses.

For the PSI concentration study, electrodes were modified in an electropolymerization solution containing 1 M aniline, 0.941 M HCl, 4 mM sodium phosphate, and 0.01% Triton X-100. The concentration of PSI was varied between 0 and 0.3 μM. Electropolymerization was carried out at +1.2 V (vs Ag/AgCl) for a fixed deposition time of 40 s.

For comparative purposes, PSI multilayer films were prepared. Using the previously published methods of Ciesielski et al.,[24] a single 60 μL aliquot of a 1.6 μM PSI solution was drop-cast onto each gold electrode. The samples were then dried under vacuum at room temperature, leaving a thin PSI film approximately 200 nm in thickness.

To evaluate the long-term stability of PAni−PSI films, three sample composite films were prepared potentiostatically, as described above, at +1.2 V vs Ag/AgCl for 40 s. These films were prepared from a solution of 1 M aniline, 0.941 M HCl, 0.3 μM PSI, 4 mM sodium phosphate, and 0.01% Triton X-100. Three traditional PSI films (∼200 nm thick) were also prepared, as described above, for comparison to the PAni−PSI composites in the long-term study.

Film Characterization. Scanning electron microscopy (SEM) images were collected with a Hitachi S4200 high-resolution scanning electron microscope. The film thickness of each sample was determined using stylus profilometry, where the average step height between the underlying gold and top layer of the PAni−PSI film was recorded using a Veeco Dektak 150 stylus profilometer.

Electrochemical Analysis. The photoactivity of PAni controls, PAni−PSI composite films, and PSI multilayers were evaluated using photochronoamperometry with a CH Instruments 660A electrochemical workstation with a Faraday cage, equipped with a three electrode setup containing a platinum mesh counter electrode and Ag/AgCl (3 M KCl) reference electrode. This three-electrode electrochemical setup allows for the evaluation of the anodic half-reaction

DOI: 10.1021/acsami.5b01065
ACS Appl. Mater. Interfaces 2015, 7, 9328−9335

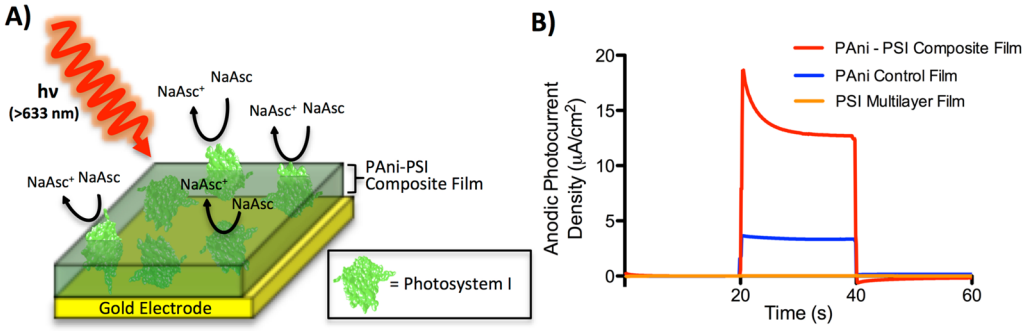

Figure 1. (A) Schematic cross section of a PAni–PSI composite film deposited onto a planar gold electrode. Sodium ascorbate (NaAsc) acts as a sacrificial electron donor for these films. Upon illumination of the composite film, an electron is promoted within PSI from the internal P700 center, and is passed to a stromal side iron–sulfur cluster, F_B. The polymer accepts an electron from PSI's reduced iron–sulfur cluster and the aqueous mediator, NaAsc, donates an electron to the oxidized $P700^+$ site. (B) Sample current–time plots for a PAni–PSI composite film, PAni film containing no PSI, and a traditional PSI multilayer film of similar thickness (~180 nm). Electrochemical analyses were performed in aqueous media containing 5 mM sodium ascorbate, 250 μM DCPIP, and 100 mM KCl as supporting electrolyte. In every trial, each sample was held at its dark open circuit potential, and illuminated from 20 to 40 s.

occurring at the working electrode independent of the platinum mesh auxiliary (counter) electrode.

Photochronoamperometry experiments were carried out in 100 mM KCl (Sigma-Aldrich) with 5 mM sodium ascorbate (Sigma-Aldrich) as an electron donor and 250 μM 2,6-dichlorophenolindophenol (DCPIP) (Sigma) to catalyze the turnover of the sodium ascorbate electrolyte. The potential of the working electrode was set to the measured dark open circuit potential. The current response was then measured upon illumination of the sample with a 250 W light source equipped with a 633 nm high pass filter (Leica KL 2500 LCD lamp). For each chronoamperometry trial, the reported steady state photocurrent was sampled 10 s after initial illumination. External quantum efficiency was calculated for the best performing PAni–PSI composite films based on maximum photocurrent density. The calculation is shown in eq 2.

In the case of the long-term stability study, the photocurrent of each replicate was sampled daily over the course of 2 weeks in order to monitor the day-to-day change in photocurrent.

Quantification of PSI in PAni Film. PAni/PSI films were grown electrochemically at +1.2 V for 40 s on gold electrodes, from a solution of 1 M aniline, 0.941 M HCl, 0.3 μM PSI, and 4 mM phosphate buffer, Pristine PAni films were grown in an identical manner, but in the absence of PSI. Following polymerization, films were dissolved in a minimal amount of concentrated nitric acid (Fisher, TraceMetal Grade), and then diluted to 5% nitric acid with 18.2 MΩ·cm deionized water.

Samples were then analyzed for iron using a PerkinElmer Optima 7000 inductively coupled plasma optical emission spectrometer, calibrated for iron emission at 238.204 nm. For quantification, a three-point calibration was constructed from Fe standards (SPEX CertiPrep) ranging from 0–50 ppb in 5% nitric acid.

RESULTS AND DISCUSSION

Photoelectrochemistry. To ensure that the PSI super-complexes were entrapped and had retained photoactivity following electropolymerization, photochronoamperometry was performed. Figure 1A depicts a cross section of the composite film containing entrapped PSI within the conductive polymer network.

Figure 1B represents the typical photoresponse for a PAni–PSI composite film (shown in red) with an overlay for a PAni control film (shown in blue). For comparison, a PSI multilayer film of comparable thickness was prepared (shown in orange). The photocurrent density of 0.03 μA cm^{-2} produced by the traditional multilayer pales in comparison to the PAni–PSI composite film. The PAni–PSI composite film yields a dramatic increase in photocurrent density over the multilayer assembly.

Polyaniline has been studied in organic thin-film solar cells as a hole-conducting material,[25] and the photoactivity observed in this study is in agreement with such behavior. Photoexcitation in the red-region and near-IR promotes electrons into the polaron band of PAni, creating a bipolaron (leading subsequently to two delocalized polarons) in the conductive film network.[26] The delocalized positive charges remaining on the polymer backbone act as strong electron acceptors, thus requiring the rapid donation of electrons from another material (i.e., PSI or sodium ascorbate) to sustain steady photocurrent output in a solar device.

In the PSI-loaded samples, illumination results in photo-activated charge separation at the internal P700 site, which drives an electron through the protein until it reaches the iron–sulfur cluster located on the stromal side of PSI. This process is depicted in the potential energy diagram of Figure 2.

In this system, to prevent effectively charge recombination within the protein, sodium ascorbate acts as a sacrificial electron donor by donating an electron to the $P700^+$ hole. From the rapid decay in photocurrent occurring immediately after initial

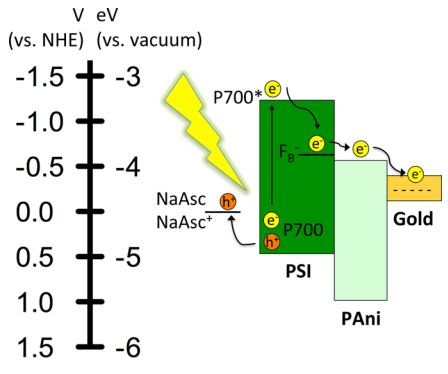

Figure 2. Potential energy diagram indicating the energy alignment of the PAni–PSI composite system. When illuminated, exciton formation and charge separation occur at the P700 site, from which the electron is passed via internal mediators until reaching the conductive PAni and subsequently the underlying gold anode. PSI cofactor energies were previously reported in ref 1, and the band energies of PAni were determined experimentally via voltammetry.

DOI: 10.1021/acsami.5b01065
ACS Appl. Mater. Interfaces 2015, 7, 9328–9335

illumination (Figure 1B) it is clear that mediator diffusion is the limiting factor in this system. This rapid decay can be modeled as Cottrell-like behavior, resulting from a diffusion-limited system. From the reduced iron–sulfur cluster, F_B^-, the electron is accepted by the PAni network and traverses through the film until it reaches the gold substrate electrode, resulting in an anodic photocurrent. The consistent polarity of the photocurrent between PSI-loaded films and PAni films indicates that the protein is acting synergistically with the polymer network to create a photoactive, biohybrid composite film capable of producing a significant enhancement in photocurrent density.

The process of electrochemical polymerization produces relatively smooth films, which can be characterized using scanning electron microscopy (SEM). Images of a pristine PAni film and PSI-loaded PAni film are presented in Figure 3. As

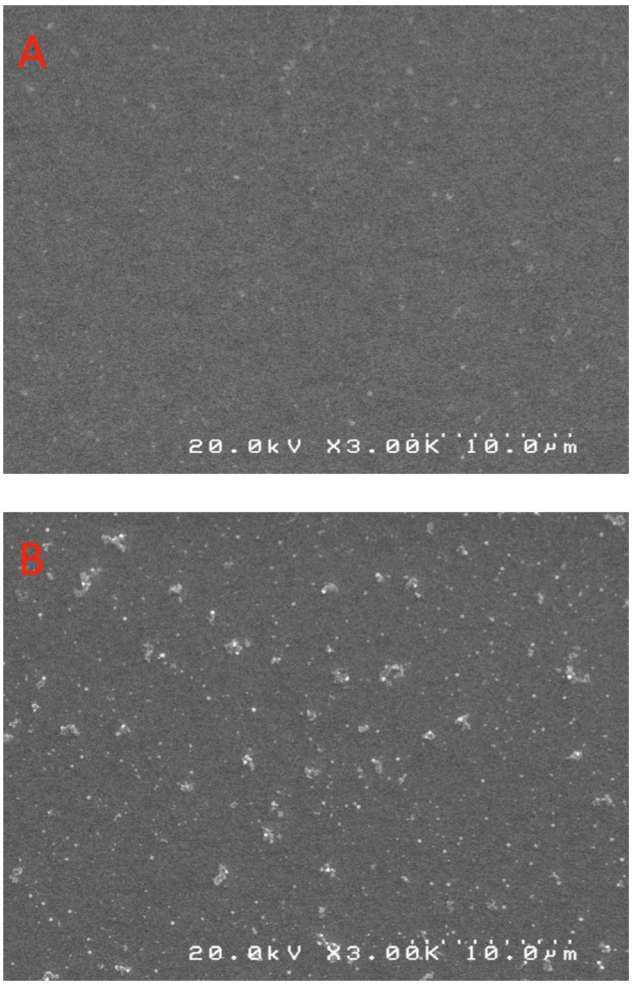

Figure 3. (A) SEM image of pristine PAni film prepared via electropolymerization. (B) SEM image of PAni/PSI composite film prepared via the electrochemical copolymerization of aniline and PSI.

expected, the pristine film is smooth and generally featureless; however, under the same preparation conditions, the film prepared in the presence of solubilized PSI resulted in an observable increase in roughness based on the encapsulation of protein in the polymer network.

Present in the PAni/PSI film (Figure 3B), but not the pristine PAni (Figure 3A), are a large number of bright clusters, attributed to the embedded PSI protein aggregates in the film. The incorporation of this iron–sulfur containing protein, into a conductive organic film has resulted in a larger quantity of reflected electrons observed by the SEM. The size of these clusters is approximately 50–500 nm. The dimensions of extracted PSI are predicted to be 8.5 × 12 nm as estimated by previous studies,[27−29] thus a small degree of protein aggregation has occurred during the entrapment process.

Due to the potentiostatic deposition method utilized in the preparation of these films, we can study the affect of film thickness on the total photocurrent output simply by modulating the polymerization time of the composite films. Figure 4 depicts this relationship as pristine PAni films (shown in blue) and PAni–PSI composite films (shown in red) were prepared using polymerization times ranging from 10 to 120 s.

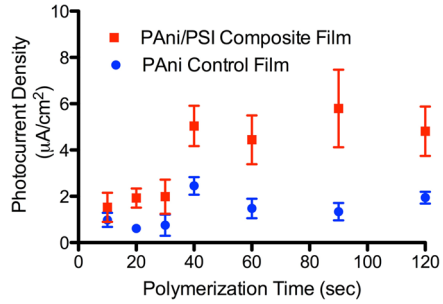

Figure 4. Effect of polymerization time on photocurrent for PAni–PSI composites (Red) (prepared from a fixed PSI concentration, 0.3 μM) and PAni control films (Blue) with no PSI. Each data point represents the average and standard error of six replicates sampled 10 s after initial red light illumination in an electrolyte solution of 100 mM KCl, 5 mM sodium ascorbate, 250 μM DCPIP.

As expected, an enhancement in observed photocurrent occurs as the polymerization time increases. Over the polymerization times of 10–30 s, photocurrent output is low, approximately 2 μA cm^{-2}, likely attributed two key factors: the marginal optical absorbance of the thin film and the minimal quantity of entrapped PSI over the brief polymerization time. As polymerization time is increased to 40 s, the photocurrent output of the composite film increases dramatically to ~5 μA cm^{-2}, indicating that (in comparison to the shorter polymerization times) either a larger quantity of protein has been entrapped or the optical density of the film is increasing as a result of film growth.

To better understand this system, it becomes important to construct a model by which polymerization time affects the film thickness of PAni. A comprehensive study was performed to correlate polymerization time to a coupled film thickness. As presented in Figure 5, it can be observed that rapid film growth occurs linearly from 10 to 40 s until a terminal thickness of approximately 200 nm is reached.

Over the 10–40 s span in Figure 5 we are able to utilize linear regression analysis to accurately construct a growth equation for PAni films, as depicted below in eq 1, where t is the polymerization time in seconds.

$$\text{film thickness (nm)} = (5.2 \pm 0.4)t - 32 \pm 12 \quad (1)$$

The terminal thickness achieved for this system is attributed to several factors including the high monomer and surfactant concentrations in the polymerization solution. Alternatively, the adoption of potentiometric polymerization methods should allow for thicker PAni films, as previously demonstrated in several studies using a variety of electrode materials.[30,31] It is

DOI: 10.1021/acsami.5b01065
ACS Appl. Mater. Interfaces 2015, 7, 9328–9335

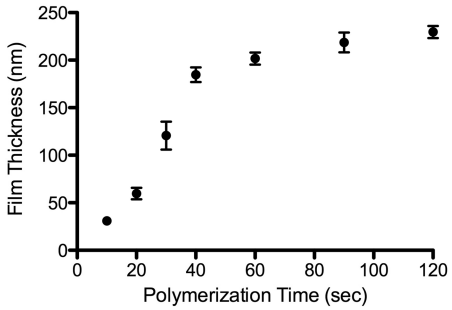

Figure 5. Correlation of potentiostatic polymerization time and thickness of PAni–PSI films. Error bars represent the standard error for three composite film samples at each deposition time.

also worth noting that the time associated with PAni–PSI film preparation is significantly shorter than the methods, which utilized a vacuum-assisted "drop-cast" method requiring at least 15 min of deposition time per ~400 nm layer of protein.[24]

After analyzing the data for film thickness with polymerization time and photocurrent output with polymerization time, it becomes apparent that the photocurrent generation of these composites follows closely with the film growth mechanism of the PAni. This is particularly evident in low photocurrent density for the 10–30 s samples, and the plateau in photocurrent density of the thickest composite films prepared in this study, approaching the terminal 200 nm thickness. At times below 40 s, the preparation time is too short to entrap an appreciable amount of solubilized PSI, thus minimal currents are observed that barely outperform the PAni controls. However, beyond this 40 s threshold, films are considerably thicker and have more time to envelope the protein in this conductive network.

After the relationship between film thickness and polymerization time was explored, the effect of PSI concentration present in the aniline solution during electropolymerization was optimized (Figure 6). For this experiment, a single deposition time was selected, 40 s (at +1.2 V vs Ag/AgCl) corresponding to a film thickness of 185 ± 13 nm at each concentration of PSI.

A rise in photocurrent density occurs as the protein concentration in the deposition solution is increased until a maximum is reached at 0.1 μM PSI. Shortly after reaching that maximum, the net photocurrent response plateaus, which identifies that above this critical concentration threshold the PSI uptake does not increase. Specifically, beyond the 0.1 μM concentration threshold the photocurrent output is dictated by the time-dependent entrapment and film growth, but not the overall PSI concentration in the polymerization solution surrounding the electrode.

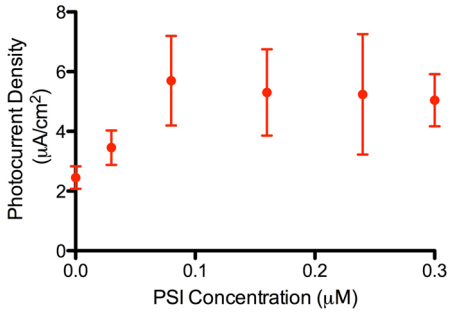

Figure 6. Effect of PSI concentration on the anodic photocurrent density of PAni–PSI composite films. Steady state photocurrent was sampled 10 s after initial red light illumination. Data points and error bars represent the average and standard error for six replicates at each PSI concentration.

After the best performing PAni–PSI electrode optimized for film thickness and initial PSI concentration was identified, the external quantum efficiency (EQE) of this film was explored. The EQE is a useful value for analyzing the performance of photoactive materials by directly correlating the electron generation (or current density) relative to photon flux incident on the substrate. In this case, we can determine the EQE for the best performing PAni–PSI film from the photocurrent output of 5.0 ± 0.9 μA cm^{-2} produced at a red light intensity of 189 mW cm^{-2}. Using these parameters, external quantum efficiency was calculated, as shown below in eq 2:

$$\frac{\text{photocurrent electrons}}{\text{incident photon flux}} \times 100 = \frac{\text{current density (A cm}^{-2})/e}{\text{power density (W cm}^{-2})/E_\lambda(J)} \times 100 \quad (2)$$

where e is the elementary charge and E_λ is the photon energy, at 633 nm. Thus, the EQE for our films was calculated to be 0.0052 ± 0.0009%. Although, other devices have reported efficiencies approaching 0.1% by relying heavily on the photovoltaic properties of semiconducting substrates,[32] the efficiency reported in the PAni–PSI film is comparable to the previously calculated values for thick PSI multilayer films on gold electrodes,[24] while operating with a PAni–PSI active layer that is 10-fold thinner than a PSI multilayer film.

Although the photocurrent output and efficiency produced in these newly developed PAni–PSI films fall short of the current benchmark performance of PSI multilayers on p-Si electrodes (approximately 200 μA cm^{-2} when normalized for mediator concentration),[33] our method presents superior advantages in reduced cost and film preparation time. PAni–PSI films do not rely on expensive, high-purity silicon wafers or a thick protein layer of nonspecifically bound PSI to generate photocurrent. In addition to providing a novel method for the assembly of large molecular weight proteins into conductive polymer films, we have now produced a new completely organic, composite material that can be interfaced with other electronic materials to create next generation solar devices that are low-cost, scalable, and stable.

In addition to the electrochemical analyses presented above, it becomes necessary to analytically quantify the amount of protein entrapped during the electropolymerization process. Based on the known stoichiometric ratio of Fe atoms (found in iron–sulfur clusters F_X, F_A, and F_B) to PSI, inductively coupled plasma optical emission spectroscopy (ICP-OES) was able to correlate trace amounts of Fe entrapped in the PAni/PSI composite films to a PSI protein density in the film (Figure 7). In this study, the best performing PAni/PSI films, prepared from 40 s polymerization in a solution containing 0.3 μM PSI, were digested in nitric acid and analyzed for Fe content.

By quantifying the Fe content through its unique atomic emission, the stoichiometric ratio of Fe to PSI (12:1) was used to quantify the amount of PSI in each film. Further, using the film radius and thickness (185 nm), a cylindrical volume model was used to calculate a protein density in each film; 14.5 ± 2.7 nmol cm^{-3} for the PAni/PSI film, and 0.4 ± 0.7 nmol cm^{-3} for the pristine PAni film. For comparison, a well-packed

DOI: 10.1021/acsami.5b01065
ACS Appl. Mater. Interfaces 2015, 7, 9328–9335

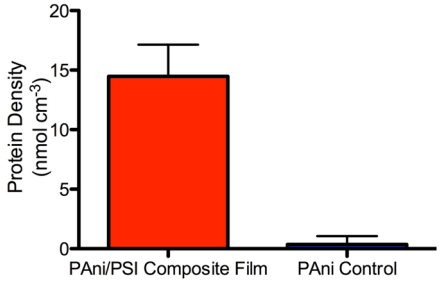

Figure 7. PSI protein density for PAni/PSI composite film (red) and PAni control film (blue), as determined by Fe elemental analysis with ICP-OES. Error bars represent the standard error of three replicates.

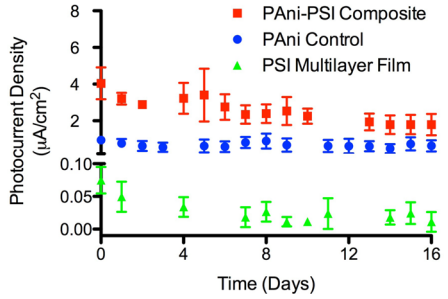

Figure 8. Long-term performance of PAni–PSI composite films, as well as unmodified PAni films and traditional PSI multilayers. Each data point represents the average and standard error of three replicates for their respective sample types. Photocurrent was sampled daily, 10 s after initial red light illumination while each working electrode was held at its dark open circuit potential.

traditional PSI multilayer film would produce a PSI density of approximately 1 μmol cm^{-3}.

With direct quantification of PSI present in the PAni–PSI composite films, we can now calculate the ensemble turnover of the enzyme within the film and ensure that appreciable activity of the enzyme is conserved. By treating our film as an enzymatic system, dictated by Michaelis–Menten kinetics,[14] we may calculate turnover frequency, where k_{cat} is defined as the maximum rate (photocurrent flux, C/s) contributed only from the PSI, divided by the quantity of PSI in the film (eq 3).

$$k_{cat} = \frac{V_{max}(C/s)}{\text{molecules of PSI}} \times \frac{1\text{electron}}{1.602 \times 10^{-19}\text{C}} \quad (3)$$

Thus, using the known quantity of PSI entrapped in our best performing film (as determined by inductively coupled plasma-optical emission spectroscopy, ICP-OES) and the photocurrent contribution from PSI in that film, we have calculated the turnover frequency to be 1.4 ± 0.5 electrons s^{-1} PSI^{-1}. This value is in agreement with those determined by Manocchi et al. in 2013,[34] where PSI layers were deposited onto alkanethiol-modified gold electrodes for electrochemical analysis.

In the case of traditional PSI films, on gold or *p*-doped silicon, the film durability is limited due to the fundamental nature of nonspecific, electrostatic binding of protein on the electrode surface, thus creating a potential drawback of such devices. Here we theorize that encapsulation of PSI within a conductive polymer network, as performed in this work, would provide superior performance longevity in photocurrent output over time. To address the issue of long-term film stability, the photocurrent output of PAni–PSI composite films was evaluated over 16 days (Figure 8). The long-term performance of simple PSI multilayers and pristine PAni films were also tracked over the same time span as represented in Figure 8.

From the initial sampling, the photocurrent density produced by the PSI-loaded PAni film (shown in red) was much higher than that generated by the PAni control films, or the traditional PSI multilayer films. The PAni–PSI composite film consistently yielded a steady photocurrent output, near 2 μA cm^{-2}, although a drop in photocurrent occurred following the initial photoelectrochemical evaluation on day 0. The PAni control film (shown in blue) produced marginal photocurrents, approximately 1 μA cm^{-2} over the course of the trial, which was significantly lower than the PSI-loaded PAni film during this span. For the traditional PSI film, after initial exposure to aqueous media, the protein film begins to degrade, as is expected for a multilayer of electrostatically bound protein. The photocurrent density produced by the PSI multilayer samples (shown in green) was significantly lower than that produced by the PAni–PSI films and the PAni control. From the onset of the trial, the output of the PSI multilayer films bottomed out near 0.01 μA cm^{-2}. In comparison to the traditional PSI multilayer films, the PAni–PSI composites represent nearly a 200-fold improvement in photocurrent after 2 weeks. This long-term performance indicates that polyaniline is an effective immobilization matrix for enhancing the lifetime of PSI biohybrid electrodes.

CONCLUSIONS

The PAni–PSI composite films prepared here introduce a rapid assembly method for integrating large molecular weight photoactive proteins into conductive polymer networks using mild electrochemical polymerization conditions without loss in enzymatic activity. A significant enhancement in photocurrent was observed for the PSI-loaded films over the PAni control films. The greatest enhancement was seen in the 185 nm thick PAni–PSI films prepared with 0.3 μM PSI in the polymerizations solution. These photocurrents (5.7 μA cm^{-2}) represent a vast improvement over multilayer PSI films of comparable thickness while incorporating 1000-fold less protein material, and rapidly assembling on a much shorter time scale. This research presents future avenues for work that incorporates PSI into conductive polymer networks, including the use of alternative substrate materials in biohybrid photovoltaic devices.

ASSOCIATED CONTENT

Supporting Information

Photocurrent action spectrum for a PAni–PSI composite film. The Supporting Information is available free of charge on the ACS Publications website at DOI: 10.1021/acsami.5b01065.

AUTHOR INFORMATION

Corresponding Author

*D. E. Cliffel. Fax: +1 615 343 1234. Tel: +1 615 343 3937. E-mail: d.cliffel@vanderbilt.edu.

Present Address

[§]University of Texas at Austin, McKetta Department of Chemical Engineering, 200 E. Dean Keeton St., Stop C0400, Austin, TX 78712-1589

Author Contributions

The paper was written through contributions of all authors. All authors have given approval to the final version of the paper.

DOI: 10.1021/acsami.5b01065
ACS Appl. Mater. Interfaces 2015, 7, 9328–9335

Funding
National Science Foundation and the Scialog Program from the Research Corporation for Science Advancement.

Notes
The authors declare no competing financial interest.

■ ACKNOWLEDGMENTS

We gratefully acknowledge the Vanderbilt Institute of Nanoscale Science and Engineering (VINSE) for use of the materials characterization laboratory (renovated under NSF ARI-R2, DMR 0963361) as well as financial support from the National Science Foundation (DMR 0907619), NSF EPSCoR (EPS 1004083), the Scialog Program from the Research Corporation for Science Advancement, and an American Chemical Society Division of Analytical Chemistry Summer Fellowship (G.L.). Additionally, we acknowledge Adam Ryan Travis for his assistance operating the ICP-OES and Shellie Richards for her assistance revising this paper.

■ ABBREVIATIONS

DCPIP, 2,6-dichlorophenolindophenol
ICP-OES, inductively coupled plasma optical emission spectroscopy
NaAsc, sodium ascorbate
PAni, polyaniline
PSI, photosystem I

■ REFERENCES

(1) Brettel, K.; Leibl, W. Electron Transfer in Photosystem I. *Biochim. Biophys. Acta* **2001**, *1507*, 100−114.
(2) Amunts, A.; Drory, O.; Nelson, N. The Structure of a Plant Photosystem I Supercomplex at 3.4 Angstrom Resolution. *Nature* **2007**, *447*, 58−63.
(3) Barber, J. Structure of Photosystem I. *Nat. Stuct. Mol. Biol.* **2001**, *8*, 577−579.
(4) Yehezkeli, O.; Tel-Vered, R.; Michaeli, D.; Willner, I.; Nechushtai, R. Photosynthetic Reaction Center-Functionalized Electrodes for Photo-bioelectrochemical Cells. *Photosynth. Res.* **2013**, *120*, 71−85.
(5) LeBlanc, G.; Gizzie, E. A.; Yang, S.; Jennings, G. K.; Photosystem, I. Protein Films at Electrode Surfaces for Solar Energy Conversion. *Langmuir* **2014**, *30*, 10990−11001.
(6) Ciobanu, M.; Kincaid, H. A.; Jennings, G. K.; Cliffel, D. E. Photosystem I Patterning Imaged by Scanning Electrochemical Microscopy. *Langmuir* **2004**, *21*, 692−698.
(7) Das, R.; Kiley, P. J.; Segal, M.; Norville, J.; Yu, A. A.; Wang, L. Y.; Trammell, S. A.; Reddick, L. E.; Kumar, R.; Stellacci, F.; Lebedev, N.; Schnur, J.; Bruce, B. D.; Zhang, S. G.; Baldo, M. Integration of Photosynthetic Protein Molecular Complexes in Solid-State Electronic Devices. *Nano Lett.* **2004**, *4*, 1079−1083.
(8) Ko, B. S.; Babcock, B.; Jennings, G. K.; Tilden, S. G.; Peterson, R. R.; Cliffel, D.; Greenbaum, E. Effect of Surface Composition on the Adsorption of Photosystem I onto Alkanethiolate Self-Assembled Monolayers on Gold. *Langmuir* **2004**, *20*, 4033−4038.
(9) Ciesielski, P. N.; Hijazi, F. M.; Scott, A. M.; Faulkner, C. J.; Beard, L.; Emmett, K.; Rosenthal, S. J.; Cliffel, D.; Jennings, G. K. Photosystem I-based Biohybrid Photoelectrochemical Cells. *Bioresour. Technol.* **2010**, *101*, 3047−3053.
(10) Ciesielski, P. N.; Cliffel, D. E.; Jennings, G. K. Kinetic Model of the Photocatalytic Effect of a Photosystem I Monolayer on a Planar Electrode Surface. *J. Phys. Chem. A* **2011**, *115*, 3326−34.
(11) Maly, J.; Masojidek, J.; Masci, A.; Ilie, M.; Cianci, E.; Foglietti, V.; Vastarella, W.; Pilloton, R. Direct Mediatorless Electron Transport between the Monolayer of Photosystem II and Poly(mercapto-p-benzoquinone) Modified Gold Electrode—New Design of Biosensor for Herbicide Detection. *Biosens. Bioelectron.* **2005**, *21*, 923−932.
(12) Yehezkeli, O.; Tel-Vered, R.; Wasserman, J.; Trifonov, A.; Michaeli, D. Integrated Photosystem II-based Photo-Bioelectrochemical Cells. *Nat. Commun.* **2012**, *3*, 1−12.
(13) Badura, A.; Kothe, T.; Schuhmann, W.; Rogner, M. Wiring Photosynthetic Enzymes to Electrodes. *Energy Environ. Sci.* **2011**, *4*, 3263−3274.
(14) Badura, A.; Guschin, D.; Kothe, T.; Kopczak, M. J.; Schuhmann, W.; Rogner, M. Photocurrent Generation by Photosystem 1 Integrated in Crosslinked Redox Hydrogels. *Energy Environ. Sci.* **2011**, *4*, 2435−2440.
(15) Badura, A.; Guschin, D.; Esper, B.; Kothe, T.; Neugebauer, S.; Schuhmann, W.; Rogner, M. Photo-Induced Electron Transfer between Photosystem 2 via Cross-linked Redox Hydrogels. *Electroanalysis* **2008**, *20*, 1043−1047.
(16) Heller, A., Redox Hydrogel-based Electrochemical Biosensors. In *Biosensors*, 2 ed.; Cooper, J., Cass, T., Eds.; Oxford University Press: Oxford, U. K., 2004; Chapter 1, pp 1−18.
(17) Gordiichuk, P. I.; Wetzelaer, G.-J. A. H.; Rimmerman, D.; Gruszka, A.; Vries, J. W. d.; Saller, M.; Gautier, D. A.; Catarci, S.; Pesce, D.; Richter, S.; Blom, P.; Herrman, A. Solid-State Biophotovoltaic Cells Containing Photosystem I. *Adv. Mater.* **2014**, *26*, 4863−4869.
(18) Baker, D. R.; Simmerman, R. F.; Sumner, J. J.; Bruce, B. D.; Lundgren, C. A. Photoelectrochemistry of Photosystem I Bound in Nafion. *Langmuir* **2014**, *30*, 13650−13655.
(19) Vidal, J.-C.; Garcia-Ruiz, E.; Castillo, J.-R. Recent Advances in Electropolymerized Conducting Polymers in Amperometric Biosensors. *Microchim. Acta* **2003**, *143*, 93−111.
(20) Foulds, N.; Lowe, C. R. Enzyme Entrapment in Electrically Conducting Polymers. *J. Chem. Soc., Faraday Trans.* **1986**, *1*, 1259−1264.
(21) Poet, P. D. T. D. Direct Electron Transfer with Glucose Oxidase in an Electropolymerized Poly(N-methylpyrrole) Film on a Gold Microelectrode. *Anal. Chim. Acta* **1990**, *235*, 255−263.
(22) Shiozawa, J. A.; Alberte, R. S.; Thornber, J. P. The P700-Chlorophyll a-Protein, Isolation and Some Characteristics of the Complex in Higher Plants. *Arch. Biochem. Biophys.* **1974**, *165*, 388−397.
(23) Baba, K.; Itoh, S.; Hastings, G.; Hoshima, S. Photoinhibition of Photosystem I Electron Transfer Activity in Isolated Photosystem I Preparations with Different Chlorophyll Contents. *Photosynth. Res.* **1996**, *47*, 121−130.
(24) Ciesielski, P. N.; Faulkner, C. J.; Irwin, M. T.; Gregory, J. M.; Tolk, N. H.; Cliffel, D. E.; Jennings, G. K. Enhanced Photocurrent Production by Photosystem I Multilayer Assemblies. *Adv. Funct. Mater.* **2010**, *20*, 4048−4054.
(25) Bejbouji, H.; Vignau, L.; Miane, J. L.; Dang, M.-T.; Oualim, E. M.; Harmouchi, M.; Mouhsen, A. Polyaniline as a Hole Injection Layer on Organic Photovoltaic Cells. *Sol. Energy Mater. Sol. Cells* **2010**, *94*, 176−181.
(26) Molapo, K. M.; Ndangili, P. M.; Ajayi, R. F.; Mbambisa, G.; Mailu, S. M.; Njomo, N.; Masikini, M.; Baker, P.; Iwuoha, E. I. Electronics of Conjugated Polymers (I): Polyaniline. *Int. J. Electrochem. Sci.* **2012**, *7*, 11859−11875.
(27) Lee, J. W.; Lee, I.; Laible, P. D.; Owens, T. G.; Greenbaum, E. Chemical Platinization and its Effect on Excitation Transfer Dynamics and P700 Photooxidation Kinetics in Isolated Photosystem I. *Biophys. J.* **1995**, *69*, 652−659.
(28) Fotiadis, D.; Muller, D. J.; Tsiotis, G.; Hasler, L.; Tittmann, P.; Mini, T.; Jeno, P.; Gross, H.; Engel, A. Surface Analysis of the Photosystem I Complex by Electron and Atomic Force Microscopy. *J. Mol. Biol.* **1998**, *283*, 83−94.
(29) Boekema, E. J.; Wynn, R. M.; Malkin, R. The Structure of Spinach Photosystem I Studied by Electron Microscopy. *Biochim. Biophys. Acta* **1990**, *1017*, 49−56.
(30) Cota, A.; Lakarda, S.; Dejeub, J.; Rougeotb, P.; Magneneta, C.; Lakarda, B.; Gauthier, M. Electrosynthesis and Characterization of Polymer Films on Silicon Substrates for Applications in Micromanipulation. *Synth. Met.* **2012**, *162*, 2370−2378.

DOI: 10.1021/acsami.5b01065
ACS Appl. Mater. Interfaces 2015, 7, 9328−9335

(31) Plesu, N.; Kellenberger, A.; Mihali, M.; Vaszilcsin, N. Effect of Temperature on the Electrochemical Synthesis and Properties of Polyaniline Films. *J. Non-Cryst. Solids* **2010**, *356*, 1081−1088.
(32) Mershin, A.; Matsumoto, K.; Kaiser, L.; Yu, D.; Vaughn, M.; Nazeeruddin, M. K.; Bruce, B. D.; Graetzel, M.; Zhang, S. Self-Assembled Photosystem-I Biophotovoltaics on Nanostructured TiO_2 and ZnO. *Sci. Rep.* **2012**, *2*, 1−7.
(33) LeBlanc, G.; Chen, G.; Gizzie, E. A.; Jennings, G. K.; Cliffel, D. E. Enhanced Photocurrents of Photosystem I Films on p-Doped Silicon. *Adv. Mater.* **2012**, *24*, 5959−5962.
(34) Manocchi, A. K.; Baker, D. R.; Pendley, S. S.; Nguyen, K.; Hurley, M. M.; Bruce, B. D.; Sumner, J. J.; Lundgren, C. A. Photocurrent Generation from Surface Assembled Photosystem I on Alkanethiol Modified Electrodes. *Langmuir* **2013**, *29*, 2412−2419.

DOI: 10.1021/acsami.5b01065
ACS Appl. Mater. Interfaces 2015, 7, 9328−9335